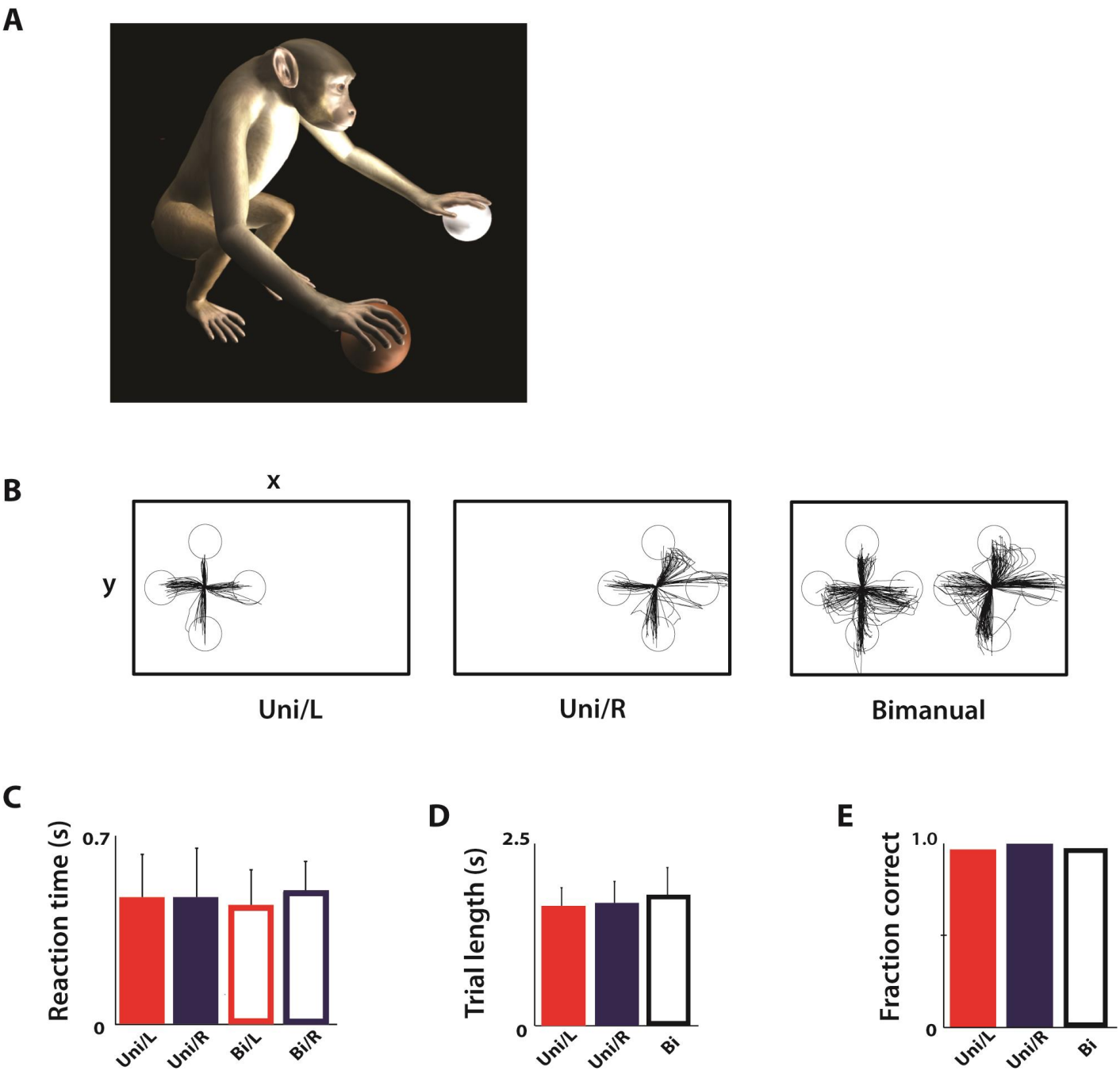

Fig. S1. Behavioral results from bimanual and unimanual joystick control experiments. (A) Virtual rhesus monkey avatar used in this study, shown here from 3rd person perspective. (B) Cursor trajectories for unimanual left, unimanual right, and bimanual trials shown as (x,y) position of the computer screen. (C) Reaction time of right and left arms during unimanual (filled bars) and bimanual (open bars). (D) Comparison of trial length for unimanual right, left, and bimanual trials (E) Comparison of fraction correct trials for each of the three trial types from a total of 354 right unimanual trials, 305 left unimanual trials, and 507 bimanual trials. All data indicates mean ± standard deviation.

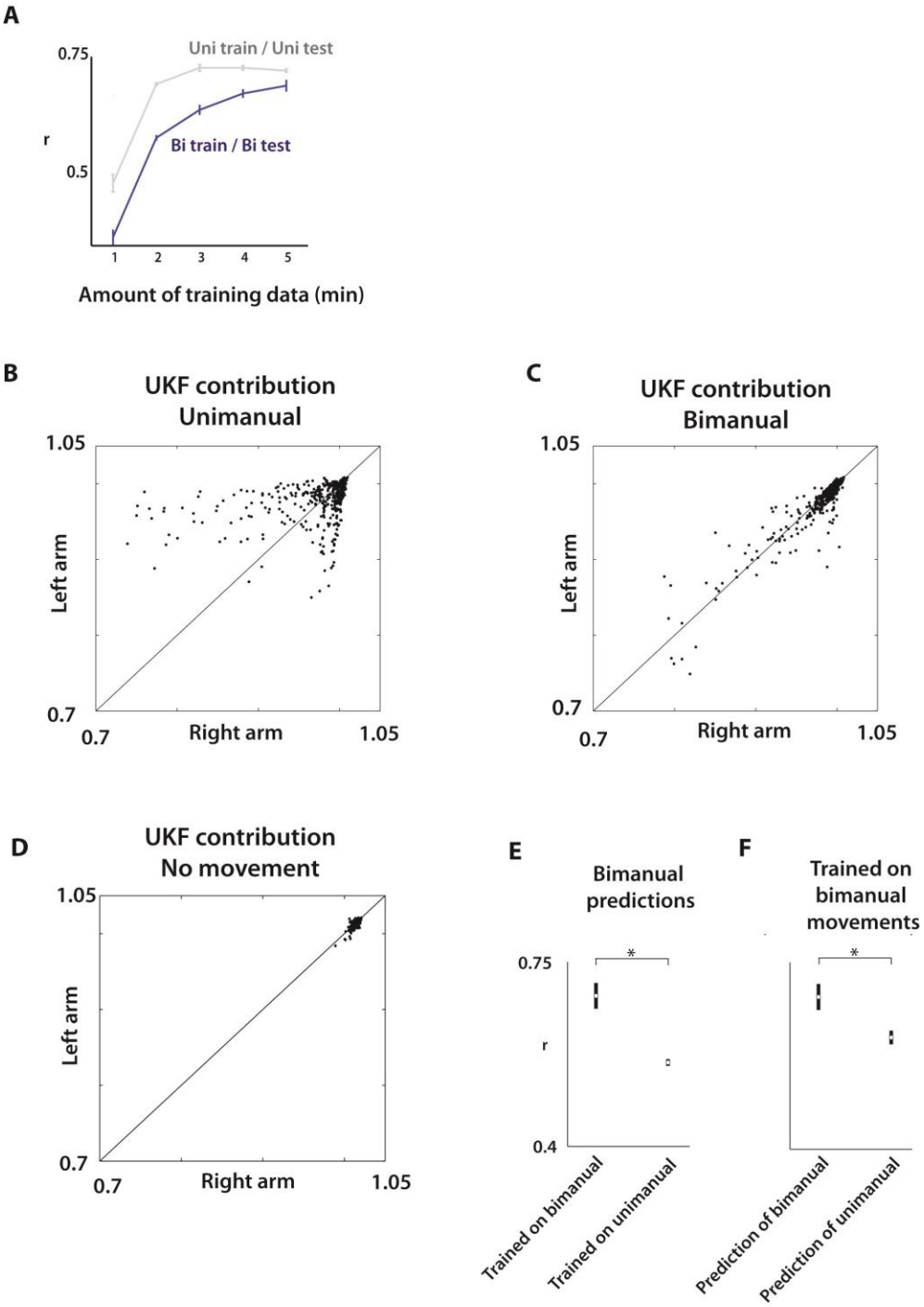

Fig. S2. Decoding performance during joystick control. (A) Prediction *r* as a function of amount of training data for both unimanual (grey line) and bimanual movements (blue lines). The decoding model for unimanual predictions was fit during unimanual trials and the model for bimanual predictions during bimanual trials. (B-D) Unscented Kalman filter noise variance terms fit on movements of left and right arms during unimanual (B), bimanual (C), and unattempted (D) trials of the same session. Values further below 1 indicate a stronger neural tuning to the predicted arm. Solid line drawn along y=x line, where both arms are represented equally. (E) Prediction of bimanual movements with training data drawn from bimanual or unimanual trials. (F) Prediction of bimanual or unimanual movements with a model trained on only bimanual trials. Data shown: mean±S.E.M.

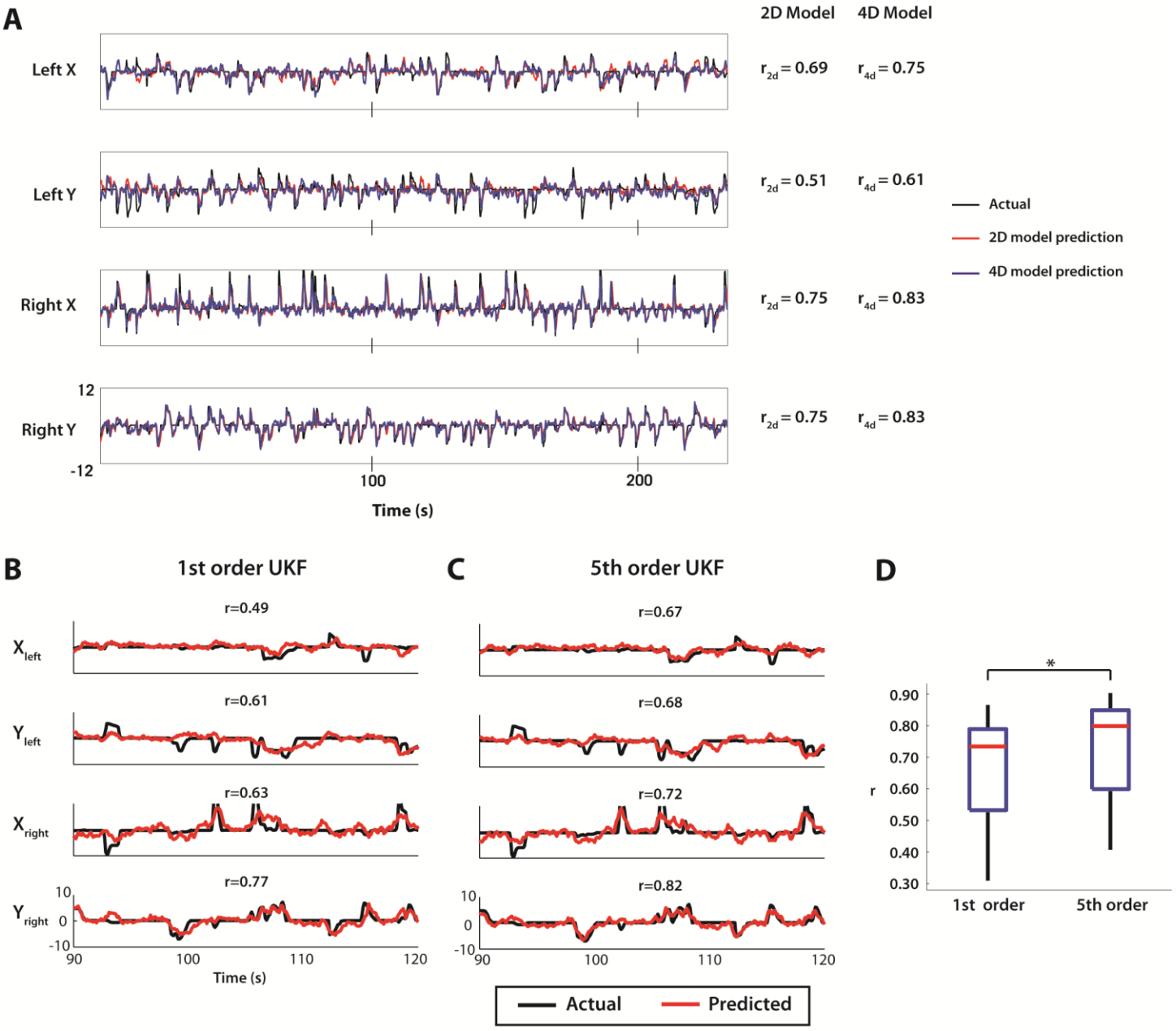

Fig. S3. Improvements to UKF model. (A) Bimanual x- and y-position predictions using 2D (red) and 4D (blue) quadratic tuning models. Black traces denote actual (x,y) position of cursor during the active bimanual experiment. The decoding strategy was otherwise equivalent for both models. 2D and 4D prediction *r* shown to right of each panel. (B-C) Comparison of the 1st (B) and 5th (C) order UKF model predictions of left arm x- and y-position and right arm x- and y-position during a 30 second window of an experiment. Prediction performance *r* is shown above each window. (D) Comparison of 1st and 5th order prediction performance distribution generated by cross-validation methods. * indicates $p<0.01$, unpaired t-test.

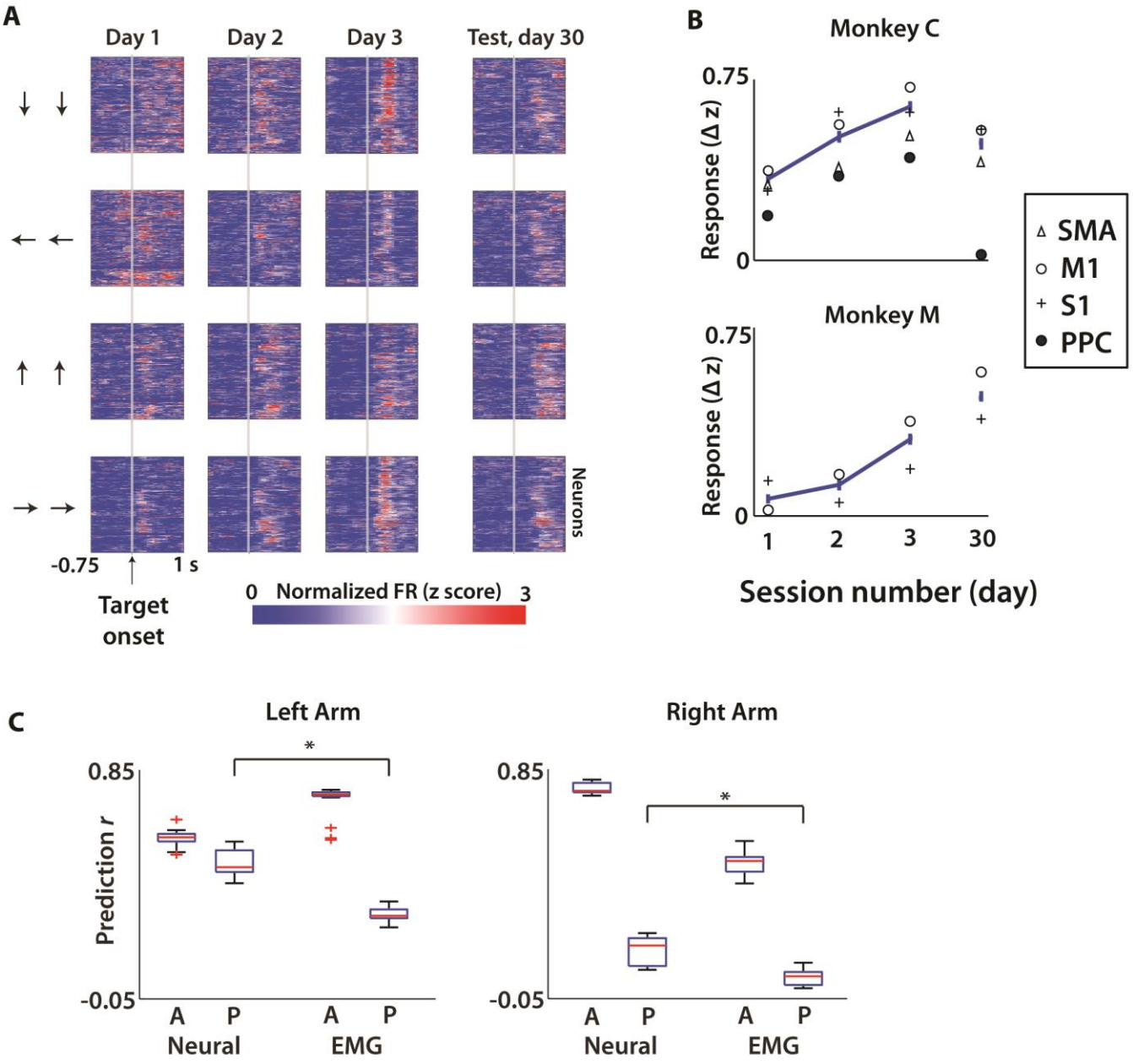

Fig. S4. Plasticity during passive observation training. (A) PETHs during passive observation for the four parallel reach directions (rows) across days 1-3 and 30 relative to initial session. Pixel color indicates normalized firing rate for each neuron. (B) Mean neural response (Δz, relative to baseline) ± standard error (blue lines) on days 1-3 and 30 for both monkey C (top) and monkey M (bottom). Shown separately are means of each cortical area. (C) Prediction *r* distributions for active (A columns) and passive (P columns) movements made using neural (left columns) and EMG activity (right columns). Analysis shown separately for left and right arm predictions. * indicates $p<0.01$, unpaired t-test)

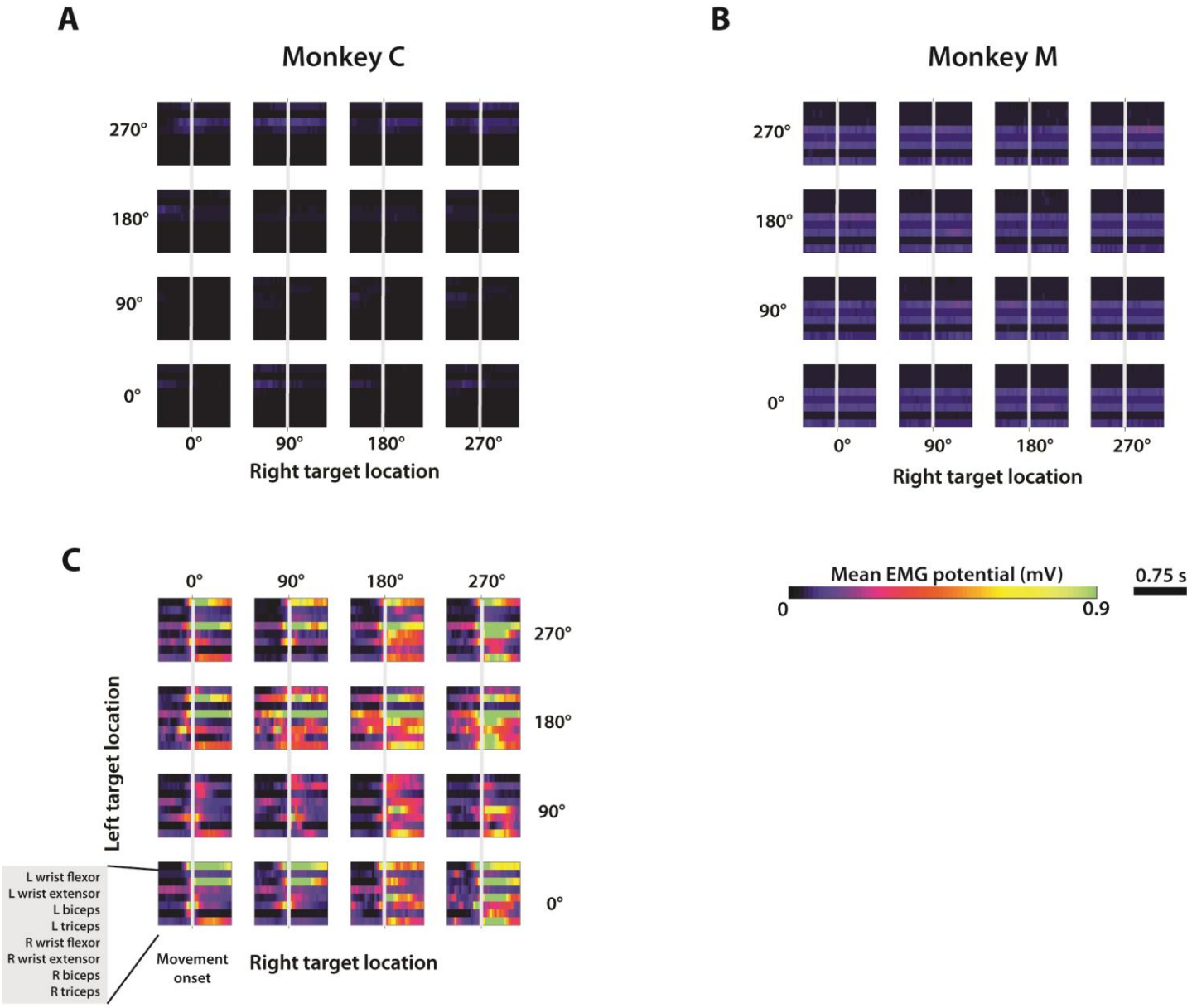

Fig. S5. Arm EMGs during passive and active trials. (A). 4x4 plot of EMG signals versus time for each of the 16 possible left/right target combinations during passive observation for monkey C. Within each panel, the 8 rows indicate 8 different muscles. Data is aligned on target appearance (grey vertical bar). Pixel color indicates amplitude of EMG signal in mV. (B) Same as (A) but for monkey M. (C) Same layout as (A) but recorded during an active bimanual session where joysticks were used by both right and left arms. Color scale below (B).

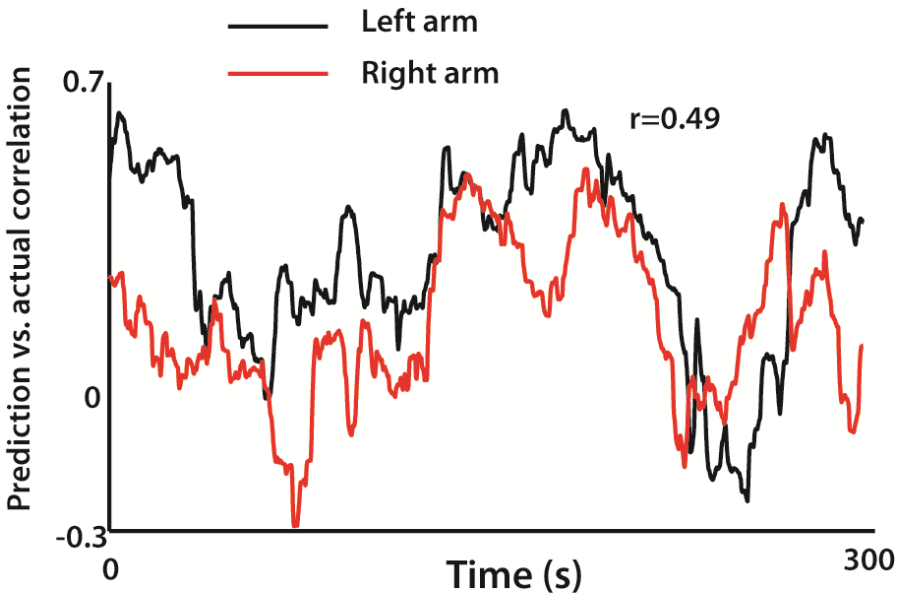

Fig. S6. Temporal changes in prediction accuracy during passive observation. Prediction *r* for left (black) and right (red) arm x-position was computed using sliding 30 second window.

	n		$\overline{\Delta z}$ Left	$\overline{\Delta z}$ Right	σ<Δz> Left	σ<Δz> Right	σ<Δz> All
L M1	187	U	0.16±0.01	0.20±0.01	0.11	0.13	-
		B	0.33±0.01		0.08	0.10	0.34
R M1	46	U	0.17±0.02	0.12±0.01	0.13	0.08	-
		B	0.19±0.01		0.08	0.09	0.12
L SMA	104	U	0.12±0.004	0.09±0.003	0.11	0.09	-
		B	0.14±0.003		0.08	0.07	0.13
R SMA	17	U	0.03±0.01	0.02±0.01	0.08	0.06	-
		B	0.03±0.01		0.05	0.06	0.06
L S1	51	U	-0.03±0.007	-0.01±0.005	0.13	0.09	-
		B	-0.02±0.003		0.06	0.06	0.10
L PPC	29	U	0.08±0.01	0.14±0.01	0.12	0.08	-
		B	0.13±0.01		0.11	0.06	0.15

Table S1

Table S1. Unimanual and bimanual modulation differences by area. (Left data column) Mean response amplitude $\overline{\Delta z}$ for unimanual left, right, and bimanual trials shown separately for each area, with neurons count *n* for each area indicated next to area name. (Right data column) Modulation depth σ(Δz) for each arm during both unimanual and bimanual movements, again separated by cortical area. The modulation depth σ(Δz) for all directions of one arm ("Left" and "Right" columns) or all bimanual directional combinations ("All" column).

Movie S1. Screen capture of bimanual center out joystick control trials. Several trials of bimanual reaches using joysticks to control the two avatar arms are shown.

Movie S2. Video of monkey performing bimanual joystick control trials using two joysticks. This video shows a side angle of the experimental setup where the arms of the monkey can be seen moving both joysticks in order to accurately control the avatar arms. Audible clicking sound is the juice reward dispensation following a correct trial.

Movie S3. Video of monkey performing bimanual BC with arms trials. Similar to joystick control setup except that the movement of avatar arms now under control of neural decoder rather than joysticks. Monkey arms are unrestrained and visible in the video. Audible clicking sound is the juice reward dispensation following a correct trial.

Movie S4. Screen capture of bimanual restrained BC trials. Several trials of bimanual reaches enacted under full brain control while both arms are fully restrained in the experimental setup.